Title: Patterns of functional and structural brain information are preserved over generations

Authors and addresses:

Yu Takagi[1,2,3*], Naohiro Okada[2,4], Shuntaro Ando[2,5], Noriaki Yahata[2,6,7], Kentaro Morita[2,8], Daisuke Koshiyama[2], Shintaro Kawakami[2], Kingo Sawada[9], Shinsuke Koike[2,10], Kaori Endo[5], Syudo Yamasaki[5], Atsushi Nishida[5], Kiyoto Kasai[2,4], Saori C Tanaka[3]

[1] Department of Psychiatry, Oxford Centre for Human Brain Activity, University of Oxford, Oxford, UK

[2] Department of Neuropsychiatry, Graduate School of Medicine, University of Tokyo, Tokyo, Japan

[3] ATR Brain Information Communication Research Laboratory Group, Kyoto, Japan

[4] International Research Center for Neurointelligence (WPI-IRCN), University of Tokyo Institutes for Advanced Study (UTIAS), University of Tokyo, Tokyo, Japan

[5] Department of Psychiatry and Behavioral Science, Tokyo Metropolitan Institute of Medical Science, Tokyo, Japan

[6] Institute for Quantum Life Science, National Institutes for Quantum and Radiological Science and Technology, Chiba, Japan

[7] Department of Molecular Imaging and Theranostics, National Institute of Radiological Sciences, National Institutes for Quantum and Radiological Science and Technology, Chiba, Japan

[8] Department of Rehabilitation, University of Tokyo Hospital, Tokyo, Japan

[9] Office for Mental Health Support, Mental Health Unit, Division for Practice Research, Center for Research on Counseling and Support Services, University of Tokyo, Tokyo, Japan

[10] University of Tokyo Institute for Diversity and Adaptation of Human Mind (UTIDAHM), University of Tokyo, Tokyo, Japan

[*]**Corresponding author**: yutakagi322@gmail.com (Yu Takagi, Ph.D.)

Competing Interests: The authors declare no competing interests.

Abstract

There is clear evidence of intergenerational transmission of life values, cognitive traits, and even aspects of daily decision making. However, the neurobiological mechanisms underlying these phenomena remain elusive. A growing amount of evidence indicates that brain information obtained using magnetic resonance imaging can predict individual differences, suggesting that the brain may also be a biological substrate of parent-child similarity. Here, by employing a large cohort dataset and machine-learning techniques, we reliably identified the brains of parents from those of their children. Identification performance was not solely driven by either functional or structural parent-child brain similarity alone; both functional and structural information contributed in a complementary fashion. Strikingly, parent-child brain similarity was found to be relevant to behavioral similarity in fundamental cognitive traits of intelligence. Our results demonstrate that patterns of functional and structural brain information are preserved over a generation, constituting a fundamental factor in parent-child similarity.

Introduction

Although all people are different, *like breeds like*. Previous studies have reported clear evidence of intergenerational transmission of socio-economic status[1], intelligence[2], personality[3], parenting style[4], and job-selection[5]. This correspondence between parents and their children is not confined to the period in which children are young and are live with their parents, but is found over the course of their lives[6]. Although various factors are clearly transferred to children from their parents, biological substrates of parent-child similarity are poorly understood.

In recent years, several studies have shown that patterns of functional connectivity (FC) during wakeful rest obtained by functional magnetic resonance imaging (fMRI) are associated with individual differences[7]. These include several cognitive domains, both in healthy people[8–13] and people with psychiatric disorders[14–17]. In parallel to research using fMRI, individual differences in brain anatomy have also been characterized and related to cognitive traits[18]. Previous studies have reported that gray matter volume (GMV) at specific locations in the brain is associated with individual differences in psychological function, both in the general population[19–21] and in people with psychiatric disorders[22,23]. Although functional and structural brain information are interrelated, they contain exclusive information that putatively characterizes distinct properties of individual differences[24].

Given that the brain has such a substantial effect on individual differences, it may be reasonable to assume that the brain is also the fundamental factor leading to parent-child similarity. However, somewhat surprisingly, no study to date has investigated whether a child's brain is more similar to their parent's brain than to another adult's brain. Although some studies have used brain information of both parents and their children[25–28], no previous study has directly tested parent-child brain similarity. Therefore, it is currently unclear how functional or structural brain properties are related to parent-child similarity. This situation has arisen, in part, because investigating the above question requires a large number of parent-child neuroimaging datasets pairs. Furthermore, such an approach requires a formal analytical framework with rigorous statistical analyses and computational resources for comparing brain similarity.

Here, we sought to understand the neurobiological substrates of parent-child similarity by combining a statistical technique and a dataset from a subsample of a large

population-based longitudinal cohort (N = 84 parent-child pairs) consisting of resting-state fMRI, structural MRI, and cognitive measures of parents and their children[29,30]. We sought to answer several questions: Do parents and their children have similar brains? If so, which brain regions contribute most to the similarity? Is the similarity solely driven by functional or structural similarity? Is neural similarity relevant to behavioral similarity?

Using a dataset consisting of parents and their children, we first quantitatively investigated parent-child brain similarity. Inspired by a recently developed classification-based approach for comparing brain similarity across different datasets[9], we proposed a framework for investigating whether parents and their children can be identified based on their brain characteristics. We first used the entire brain, then split it into sub-networks and investigated which brain networks contributed to parent-child identification. We next compared functional and structural brain information, making it possible to quantitatively evaluate how these two types of information are related to each other in terms of parent-child identification. Finally, we related parent-child brain similarity to behavioral similarity using fundamental cognitive measures of intelligence.

In the present study, we found that a child's brain obtained at age 11 was more similar to their parent's brain than to the brain of another child's parent. This effect was not solely driven by either functional or structural brain similarity: although functional and structural information exhibited comparable identification accuracy, they exhibited important differences, and played complementary roles in parent-child identification. All of the results were robustly reproduced when we used a dataset of children at age 13. Finally, the results revealed that parent-child brain similarity was relevant to parent-child behavioral similarity in fundamental cognitive measures of intelligence. Our results suggested that parent-child brain similarity may be a major neurobiological substrate of a broad range of parent-child similarities.

Results

We tested 84 pairs of parents and children who participated in the "population-neuroscience study of the Tokyo TEEN Cohort (pn-TTC)," a longitudinal study exploring the neurobiological substrates of development during adolescence[29,30]. In the pn-TTC study, brain structural, functional, and non-imaging cognitive measures were collected from children every 2 years from the age of 11 and their primary parents (Figure 1a; see *Methods: Overview of the dataset*). Here, we used three brain datasets from the pn-TTC study: children at the ages of 11 and 13, and their primary parents. Parents' brains were scanned when their children were 11 years old. The basic demographic data are shown in Table 1.

To evaluate parent-child brain similarity quantitatively, we first defined the functional and structural whole-brain patterns for each individual (Figure 1a; see *Methods: Information extraction*). For fMRI, we used a functional atlas defining 268 regions of interest (ROIs) that cover the entire brain[9,31]. The functional connectivity (FC or edge) between these ROIs was estimated using Pearson's correlation coefficient, resulting in a 268 × 268 FC matrix for each subject. As the FC matrix is symmetrical, only the strictly lower triangular part of each matrix was kept, resulting in 35,778 (= 268 × 267 / 2) unique entries. We regressed potential confounds (including total gray matter volume and head motion) out of raw signals and resulted in matrices. To further avoid the effects of motion artifacts, we employed a "scrubbing" procedure to identify and exclude any frames exhibiting excessive head motion[32]. We also obtained GMV for each ROI using T1w images, then averaged within each region. We used the same 268 ROIs as in the fMRI, resulting in a vector with a size of 268 for each subject.

To evaluate brain similarity, we employed a pairwise classification approach using parent-child pairs (Figure 1b), inspired by a recently proposed approach for identification of the same individual[9]. First, the FC or GMV from a child is randomly selected from all children in the sample. Next, two parents, including the child's own parent and a randomly selected parent, were selected. If the Pearson's correlation coefficient for the own parent is higher than that for another child's parent, the result is recorded as a correct parent-child identification. The process was repeated 1,000 times for calculating identification accuracy. We performed 1,000-times bootstrapping for estimating 95% confidence intervals of accuracy by randomly subsampling 90% of the subjects in each iteration. To determine whether identification performance was achieved at above-chance levels, we used 1,000-

times permutation testing to generate a null distribution by randomly shuffling the parent-child mapping.

Whole-brain identification

Parent-child identification was performed using the whole-brain FC and GMV. When we used a dataset of children at age 11, the accuracies were 64.99% for FC (estimated via 1,000-times bootstrapping; 95% CI = [61.7, 68.7]) and 66.52% for GMV (95% CI = [63.5, 69.7]) (Figure 2a). When we used a dataset of children at age 13, the accuracies were 68.02 for FC (95% CI = [65.1, 70.7]) and 70.54% for GMV (95% CI = [67.6, 73.4]) (Figure 2b). Given that almost all parents in the sample were female (81 mothers among 84 parents), we split all children into male (N = 45) and female (N = 39) groups, then conducted the same procedure for each group. Although females had slightly higher accuracy, particularly for FC, the two groups exhibited qualitatively similar results (Supplementary Figure 1).

We next assessed the importance of information for identification performance of specific edges for FC and regions for GMV, respectively (Figures 2c, 2d, 2e, and 2f). To quantify the extent to which different edges and regions contribute to identification, we derived two measures: the differential power (DP) which calculates how characteristic an edges and regions tend to be, and the group consistency (Φ) which quantifies edges and regions that are highly consistent across all parent-child pairs in a dataset[9] (see *Methods: Identification analysis*). For visualization purposes, we show the structural locations of DP and Φ in the 99.75th and 90th percentile, for edges (FC) and regions (GMV) respectively. For both FC and GMV, significant edges or regions tended to be distributed across the entire brain. This pattern was stable across a range of thresholds (Supplementary Figure 3). Note that, for visualization purposes, we excluded the brainstem from the figure for GMV because all regions in this area had extremely high Φ values, possibly because of the much lower magnitudes of signals compared with the other regions (Supplementary Figure 4).

Given that head motion confounds analyses of FC[32], we confirmed that qualitatively similar results were obtained when we excluded parent-child pairs whose children's head movements were in the top 25%, either at age 11 or at age 13, resulting in the inclusion of 41.25% of the total sample (Supplementary Figure 2). We also confirmed that we could not conduct parent-child identification on the basis of the distribution of their frame-to-frame motion during fMRI scans[9] ("MOTION" column in Supplementary Table 1). Thus, it is unlikely that the identification power of FC was based on idiosyncratic patterns related to motion in

the scanner.

Network-based identification

Having determined that parent-child brain identification could be successfully conducted, we further investigated the contributions of specific networks to this similarity. We grouped the whole regions into 10 sub-networks[33] (Figure 3a), and subsequently performed identification analyses using only the edges and regions from a given network.

For FC, medial frontal and frontoparietal networks led to high accuracies (Figure 3b). In contrast, for GMV, default mode, subcortical, cerebellum and visual networks led to high accuracy (Figure 3c). To further assess the importance of each network, we next assessed identification performance using between-network pairs of edges. We observed that edges between the medial frontal–frontoparietal networks and medial frontal–motor networks resulted in higher accuracies than the other between-network pairs (Figure 3d).

Function and structure have complementary information

Although FC and GMV revealed comparable performance in the above analyses, it remains unclear whether they contain similar information in terms of identification. This raises the following question: if parents and their children exhibit similar patterns of structural brain information, do they also exhibit similar patterns of functional brain information? To test this question, we investigated the relationship between parent-child similarity defined by FC and that of GMV. We found that, when we used whole-brain information, Pearson's correlation coefficients between similarities defined by FC and GMV were relatively low: 0.08 (child at age 11–parent), and 0.21 (child at age 13–parent). When we split the whole brain into 10 sub-networks (see Figure 3a) and calculated similarities for each sub-network, correlations were still low for all networks: 0.02 ± 0.10 (child at age 11–parent; mean ± s.e.m), and 0.08 ± 0.07 (child at age 13–parent). Thus, although the identification performance of FC and GMV was similar, their characteristics were dissimilar (see Supplementary Figure 5 for all results).

Given that FC and GMV appear to contain independent information, we further investigated whether they contain complementary information for identification. To test this question, we conducted identification using both FC and GMV simultaneously by concatenating the two vectors (hereafter referred to as "COMB"). We used machine-learning techniques for automatically determining the weights of each dimension of FC and GMV,

because it was not obvious how different types of information contributed to identification (see *Methods: Identification analysis*). Briefly, we applied canonical correlation analysis (CCA) [34] to the datasets of parent-child pairs. CCA can identify an optimal linear transformation matrix for maximizing the correlation between different pairs of matrices (in our case, parent-child pairs). Before CCA, we also applied principal component analysis (PCA) to the matrices of FC and GMV separately, a conventional method for denoising datasets in neuroimaging[11,15,35]. All weights and hyperparameters related to CCA and PCA were determined through a nested-cross validation procedure, and accuracies were calculated based on a hold-out test dataset. Table 2 shows that COMB with CCA achieved the best identification performance when we used whole-brain data (accuracy = 82.54, 95% CI = [78.79, 86.24]) and achieved the best performance for almost all sub-networks (19 of 22 networks). Even without CCA, COMB tended to achieve the highest accuracies (14/22) compared with function (3/22) and structure (5/22) alone. We also applied CCA to FC and GMV separately and confirmed that COMB with CCA still achieved the best performance in almost all sub-networks (18/22, see Supplementary Table 1). Overall, these results suggest that neither function nor structural brain information was solely responsible for enabling parent-child identification: rather, they contained complementary information in terms of identification.

Relationship between brain similarity and behavioral similarity

The results described above indicated that parents and their children exhibit similar functional and structural brain information. However, this finding does not clarify whether parent-child neural similarity is meaningful or relevant to parent-child *behavioral* similarity. If so, this would suggest that parent-child brain similarity constitutes a major biological substrate of their behavioral similarity. To investigate this question, we defined “behavioral similarity” as the difference in fundamental cognitive traits of intelligence between a parent and their child (see *Methods: Behavioral correlation*). We also defined “neural similarity” as the correlation coefficient between brain information of parents and their children. For brain information, we used a combination of FC and GMV data with CCA, which achieved the highest identification accuracies (“COMB [CCA]” column in Table 2). We averaged neural similarity of children at age 11 and age 13 to improve sensitivity.

We found that neural similarity defined at DMN was positively correlated with behavioral similarity (Figure 4a; see Supplementary Table 2 for all networks). Specifically, parent-child pairs exhibiting high neural similarity also exhibited high behavioral similarity (Spearman’s rank correlation = 0.3861, 95% CI = [0.3232, 0.4578], estimated via 1,000-times

bootstrapping; $P < 0.05$, 1,000-times permutation test; Bonferroni family-wise error rate corrected for 11-times statistical testing [10 sub-networks and the whole brain]). It should be noted that DMN exhibited the highest accuracy when averaging identification accuracies obtained by both FC and GMV across children at age 11 and 13 (DMN had an average accuracy of 62.54%, calculated by averaging 62.29% [FC, child at age 11], 57.76% [FC, child at age 13], 64.75% [GMV, child at age 11], and 65.45% [GMV, child at age 13]; see Table 2). We confirmed that we obtained similar results when we calculated the partial correlation, which considers head motion as a confounder (partial R = 0.3772, 95% CI = [0.3054, 0.4552], $P < 0.05$, 1,000-times permutation test; Bonferroni family-wise error rate corrected; see Supplementary Figure 6).

Discussion

The present study revealed, for the first time, that children and their parents exhibit similar functional and structural brain information patterns. We employed a rigorous predictive framework and the richest number of functional and structural neuroimaging pairs of children and their primary parents (N = 84 parent-child pairs)[29,30]. Although both functional and structural brain information achieved a comparable level of identification, their characteristics were different but complementary in terms of identification. All results obtained using children's data at age 11 were robustly replicated using children's data at age 13. Parent-child brain similarity was also relevant to parent-child behavioral similarity measured by fundamental cognitive measures of intelligence. Taken together, our results clearly demonstrate that the brain is one of the fundamental factors determining parent-child similarity.

Our results revealed that, despite the substantial differences between parents and their children, including environment and age, their brains are sufficiently similar that we were able to successfully identify parent-child relationships based on brain characteristics, with up to 82.54% accuracy (Table 2). Although parent-child similarity has been investigated in various research fields, including developmental psychology, educational psychology, and economics, to the best of our knowledge no previous study has investigated whether a child's brain is more similar to their parent's brain compared with the brain of another child's parent. The current results also revealed that parents and their children also have similar brain properties. Although some previous neuroimaging studies have tested parents and their children, they have not investigated parent-child brain similarity because of the small sample size and lack of an analytical framework[25–28]. The present study is the first to investigate this important question by employing a recently developed predictive framework[9] and a rich parent-child brain dataset.

For both function and structure, the contributed brain regions tended to be broadly distributed across the entire brain when we used whole-brain information (Figure 2c-2f), in stark contrast to previous identification studies within same individual, demonstrating that constrained networks were highly discriminative or highly consistent across individuals[9,33]. Although this tendency was retained when we only used the edges or regions within sub-network, we observed slightly different contrasts between functional and structural information (Figure 3b–3d and Table 2). Specifically, for function, the medial frontal, and

frontoparietal areas, which are known to be networks related to higher cognitive function, revealed the higher identification accuracies than structure. In contrast, for structure, visual, subcortical, and cerebellum networks exhibited higher identification accuracies than function. This contrast is interesting because the prefrontal cortex is one of the last regions of the brain to reach maturation, exhibiting development until approximately 25 years of age, whereas subcortical regions reach maturation earlier[36].

We confirmed that our results were not solely driven by structural or functional similarity. The neural similarity between FC and GMV has a weak correlation (Supplementary Figure 5). In addition, by combining FC and GMV, we achieved the highest identification accuracy, of 82.54% (Table 2). These results indicate that FC and GMV are distinct, and contain complementary information for identification. Previous studies reported that function and structure contain similar information, but also distinct information[24]. One study also showed that information obtained from function and structure contain complementary information for the identification of siblings, but did not investigate the contributions of distinct anatomical brain locations[37]. The current results are not only consistent with those of previous studies but also demonstrated qualitative differences between function and structure by exhaustively investigating the contributions of each distinct anatomical brain location.

We also found that parent-child neural similarity calculated in the DMN was positively correlated with the behavioral similarity of fundamental cognitive measures of intelligence (Figure 4). This finding is intriguing because the DMN has the highest accuracy when averaging identification accuracies obtained by both FC and GMV across children at ages 11 and 13 (Table 2). Previous studies reported that an individual's intelligence scores can be predicted by FC within the DMN[9]. Intelligence measures are related to a wide range of cognitive functions, and may predict various social outcomes[38], and parent's, particularly mother's, intelligence levels are related to their child's intelligence level[39]. The current results thus suggest that parent-child brain similarity might be a major biological substrate of the broad range of parent-child behavioral similarities.

To quantitatively investigate the parent-child brain similarity, we employed a pair-wise classification approach, inspired by recently proposed approaches for individual identification[9,33]. Another line of studies has investigated brain similarity among siblings[37,40–43]. The current study is conceptually different from these previous studies, which used datasets from the same individual or siblings, and potentially addresses a more difficult problem because differences between parents and their children may be substantially larger

than differences within the same individual or between siblings with similar biological and environmental factors. However, it should be noted that, for function, the contributed functional edges were very different from the results of previous individual identification studies, which reported a strong cluster in medial frontal and frontoparietal areas[9,33,41]. For structure, only a small number of studies using GMV are comparable to the current study[44,45], and none of them investigated each network's contribution in detail.

Recent developments in cognitive neuroscience have made it possible to investigate individual differences, an issue that has been ignored for decades because of the absence of adequate datasets, analytical techniques, and computational resources. The current results shed light on the importance of investigating differences in family-level differences, not only individual-level differences. Families are not a neutral environment for identity development, but deeply affect the individual from adolescence, strongly influencing the development of a person's identity[46]. Given that the current results revealed that parental brains are similar to the brains of their children, we propose that future studies should investigate the relationships between family-level behavioral indices and family-level brain information to enable more reliable predictions of children's behavior and development. We believe our publicly available dataset will help to extend research in this direction[30].

There are several potentially interesting future questions. The first and perhaps most important question is whether parent-child brain similarity changes across children's development. Recent studies proposed a brain-based quantitative approach for investigating the trajectory of the development[47,48]. Thus, it may be valuable to investigate whether the trajectory of the parent-child brain similarity will affect the various risks faced by adolescents, including psychiatric disorders and criminal behavior. Second, insights may be gained by using genetic information to confirm the extent to which genetic factors contribute to neural similarity. We examined biological parent-child relationships in the current study. Thus, it may be valuable to test whether non-biological parents and children show the same level of brain similarity. Third, we used GMV as a structural brain measurement because a number of previous studies have investigated the relationship between GMV and various traits. However, the human brain also exhibits individual differences in white matter microstructure. Diffusion tensor imaging provides measures of white matter integrity in the brain, and has useful, but, like GMV, different information to the FC[49]. Indeed, previous studies have shown that thickness correlations partially reflect underlying fiber connections but contain exclusive information[50]. Future studies should use other types of structural information, such as

structural connectivity obtained by diffusion tensor imaging. Fourth, because our dataset mostly consisted of mothers (81 mothers among 84 parents), it may be valuable to test whether we can also identify children's fathers via brain similarity. Although we confirmed that we were able to successfully conduct identification analyses even when we used only male or female children (Supplementary Figure 1), future studies should investigate the effects of parents' sex on identification performance.

In the present study, we sought to address a critical question in social science: why are parents and their children so similar? Our analytical framework and the richness of our parent-child brain dataset made it possible to conduct the first investigation of parent-child brain similarity. The results revealed that parents' brains are relatively similar to those of their children, and that this brain similarity is relevant to behavioral similarity measured by fundamental cognitive measures of intelligence. These results suggest that the brain is a fundamental factor in parent-child similarity.

Acknowledgments

This study is the result of the projects "Science of personalized value development through adolescence: integration of brain, real-world, and life-course approaches" (16H06396, 16H06398, 16H06399) and "Adolescent Mind & Self-Regulation" (23118001, 23118002) of Grants-in-Aid for Scientific Research on Innovative Areas from the Japan Society for the Promotion of Science. We thank Hiroshi Imamizu, Ph.D., Ryu Ohata, Ph.D., Ayumu Yamashita, Ph.D., and Aurelio Cortese, Ph.D. for reviewing the draft and helpful discussions. We thank Okito Yamashita, Ph.D., and Jun-ichiro Hirayama, Ph.D. for helpful discussions. We thank Kana Inoue and Kaori Tachi for their support with data collection. We thank Giuseppe Lisi, Ph.D. for his support with code sharing. We thank Corey Horien for his support with code and data sharing.

Author Contributions

N.O., S.A., N.Y., K.M., D.K., S.Kawakami, K.S., S.Koike, K.E., S.Y., A.N., K.K., and S.C.T. recruited participants for the study and collected their behavioral and imaging data. N.O. inspected imaging data. N.Y. provided analysis codes. S.Koike, and K.K., interpreted the results and provided technical advice. S.C.T. supervised the study. Y.T. conceptualized the study, conducted the analysis, visualized the data, and wrote the manuscript. All authors reviewed the

manuscript.

Data and code availability statement

The data and code supporting the findings of this study are available from the corresponding author upon reasonable request.

Methods

Overview of the dataset

The Tokyo TEEN Cohort (TTC) study, which was launched in 2012, is a large-scale longitudinal general population-based survey to elucidate puberty development during adolescence, particularly the acquisition process of self-regulation and willingness to challenge, by focusing on the interaction between biological, psychological, and social factors[29,30]. This study was conducted as part of the population-neuroscience study of the TTC (pn-TTC) study, in which 301 early adolescents were recruited from the general population. Subjects of the pn-TTC study were subsampled from a larger subject group of the TTC study, and it was confirmed that the pn-TTC subsample was representative of the TTC study population. Written informed consent was obtained from each subject and the subject's primary parent before participation. All protocols were approved by the research ethics committees of the Graduate School of Medicine and Faculty of Medicine at the University of Tokyo, Tokyo Metropolitan Institute of Medical Science, and the Graduate University for Advanced Studies. All research was performed in accordance with relevant guidelines/regulations. The detailed methods for subject recruitment are described elsewhere[29,30]. The dataset is publicly shared upon request (http://value.umin.jp/data-resource.html).

We excluded subjects who exhibited anomalies in fMRI or T1w images. We also excluded parents who did not have either fMRI or T1w images, and children who did not have either fMRI or T1w images at age 11 and age 13. After this screening process, 84 pairs were included in the final analysis (39 female children; 81 mothers; age = 11.59 ± 0.66 for children at age 11, 13.63 ± 0.62 for children at age 13, and 43.35 ± 0.62 for parents, mean ± s.t.d).

MRI parameters

Subjects were instructed to lie supine on the bed of the MRI scanner. MRI scanning was performed on a Philips Achieva 3T system (Philips Medical Systems, Best, The Netherlands) using an 8-channel receiver head coil. Each subject underwent resting-state fMRI and T1-weighted (T1w) three-dimensional magnetization-prepared rapid gradient echo (3D-MPRAGE) sequences.

Sagittal T1w images were acquired using the 3D-MPRAGE sequence with the

following parameters: repetition time (TR) = 7.0 ms, echo time (TE) = 3.2 ms, minimum inversion time = 875.8 ms, flip angle = 9°, matrix = 256 × 256, field of view (FOV) = 256 mm × 240 mm × 200 mm, voxel size = 1 mm × 1 mm × 1 mm, slice thickness = 1 mm, number of slices = 200. The acquisition time was approximately 10 min 42 sec.

Resting-state fMRI images were acquired by a gradient-echo echo-planar imaging (EPI) sequence with the following parameters: TR / TE, 2500 ms / 30 ms; flip angle, 80°; matrix, 64 × 64; FOV, 212 mm × 199 mm × 159 mm; voxel size, 3.31 mm × 3.31 mm; slice thickness, 3.20 mm; slice gap, 0.8 mm. Each brain volume consisted of 40 axial slices and each functional run contained 250 image volumes preceded by four dummy volumes, resulting in a total scan time of 10 min 40 sec. Subjects were instructed to stay awake, to keep their minds as clear as possible, and to keep their eyes on a fixation point at the center of the screen through a mirror during scanning.

Information extraction

We used Statistical Parametric Mapping 8 (SPM8: Wellcome Department of Cognitive Neurology, http:/ /www.fil.ion.ucl.ac.uk/spm/software/) in MATLAB (MathWorks, Natick, Massachusetts) for preprocessing and statistical analyses.

Preprocessing of resting-state fMRI: Preprocessing of resting-state fMRI included slice-timing correction, realignment, co-registration, segmentation of T1-weighted structural images, normalization to Montreal Neurological Institute (MNI) space, and spatial smoothing with an isotropic Gaussian kernel of 6 mm full-width at half-maximum. To avoid the effects of head motion artifacts, we calculated framewise displacement (FD). FD is defined as the mean relative displacement between two consecutive volumes for each of the six motion parameters. We conducted the "scrubbing" procedure by removing volumes with FD > 0.5 mm, along with the previous volume and two subsequent volumes, as proposed in Power et al.[32] For each subject, a pair-wise, interregional FC was evaluated among regions of interest (ROIs) covering the entire brain. We used a functional atlas defining 268 ROIs that cover the entire brain (functional atlas from Finn et al.[9], which used the method developed by Shen et al.[31]) (this atlas can be downloaded from https://www.nitrc.org/frs/?group_id=51). The average gray matter time-course for each ROI was calculated, and then temporally filtered using a first-order Butterworth filter with a pass band between 0.01 Hz and 0.08 Hz. The time-course of each ROI was linearly regressed by the temporal fluctuations in white matter, cerebrospinal fluid, and entire brain, as well as six head motion parameters. The time-course

431 of white matter and cerebrospinal fluid were filtered using a first-order Butterworth filter with
432 a pass band between 0.01 Hz and 0.08 Hz , and white matter mask was eroded by one voxel
433 to consider a partial volume effect. All parameters were determined as done in a previous
434 work[17]. For each subject, an FC matrix between all ROIs was then calculated by evaluating
435 pair-wise temporal Pearson correlations of BOLD time courses, based only on the remaining
436 images after the scrubbing step above. Because FC matrices are symmetric, values on only
437 one side of the diagonal were kept, resulting in 35,778 unique edges (268 × 267/2). We then
438 regressed the motion and total gray matter volume and mean FD out from data matrices.

439 *Preprocessing of* structural *MRI:* T1w images were segmented into three tissue
440 classes (gray matter [GM], white matter [WM], and cerebrospinal fluid [CSF]) using a
441 segmentation approach implemented in SPM8. The segmented images (only GM) were then
442 normalized into standardized Montreal Neurological Institute space by applying a deformation
443 field in SPM8. The GMV of each ROI was extracted and averaged within that ROI. We used the
444 same 268 ROIs that were used for FC, enabling us to obtain a vector with a size of 268 for each
445 subject. Note that, although an alternative method for inter-subject registration called
446 Diffeomorphic Anatomical Registration Exponentiated Lie algebra (DARTEL) exists, we did not
447 employ it because our goal was not to conduct comparisons at the group-level. Future studies
448 should investigate whether employing another segmentation and normalization method can
449 improve identification accuracy.

450 *Motion index:* In addition to resting-state fMRI and structural MRI information, we
451 performed identification using motion estimates during resting-state fMRI to rule out the
452 possibility that successful identification using FC was driven simply by characteristic
453 movement patterns[9]. We first specified 20 bins to span {0:0.05:1} to calculate discrete motion
454 distribution vectors for each parent and child based on FD over an entire scan. These motion
455 distribution vectors were then used in the same way as the FC or GMV vectors for
456 identification purposes.

457 Identification analysis

458 We employed a pairwise classification approach using parent-child pairs (Figure 1b). During
459 identification, an input vector (further details described below) was randomly selected from
460 the children. Next, two parents, including the child's parent, were selected. If the Pearson's
461 correlation coefficient between two vectors for a parent and the parent's child is higher than
462 that between the child and another parent, it was recorded as a correct identification. This

process was repeated 1,000 times. We performed 1,000-times bootstrapping to estimate the 95% confidence interval of accuracy, subsampled 90% of the subjects in each iteration, and performed identification. We conducted the same analyses using datasets of children at age 11, or at age 13, to investigate the reproducibility and stability of our results across development. To determine whether identification accuracy was achieved at above-chance levels, we used 1,000-times permutation testing to generate a null distribution by randomly shuffling the parent-child mapping.

To determine the role of specific edges in the identification process, we quantified highly unique and highly consistent edges/regions using the differential power (DP) measure and the group consistency measure (Φ) described in detail elsewhere[9]. DP provides an estimate, for each given edge/region, of the likelihood that within-family similarity (between a parent and their child) is higher than between-family similarity (between a parent and another parent's child). To calculate the DP, the product of an edge/region value of a parent and their child was compared with the product of the same edge/region value of another parent's child. If the within-family product was higher than the between-family product across all pairs in a sample, this corresponds to a high DP value, and the edge/region is helpful in identification. To calculate the value of Φ, we multiplied a given edge/region value from a parent and their child. We did this across all edges/regions for all pairs and calculated the mean for each edge/region. Edges/regions with high Φ values are therefore high across all pairs and are not helpful for identification.

For the analyses of Figure 2, we used whole-brain FC or GMV. For the analyses of the data shown in Figure 3, we split the whole brain into 10 sub-networks and conducted the same analyses using FC or GMV within each sub-network. The definition of sub-networks was obtained from Horien et al., 2019[33].

For the analyses of Table 2 and Supplementary Table 1, we used a machine-learning approach, whereby we learned the optimal linear combination of two different types of the dataset: parents and their children. Specifically, we applied canonical correlation analysis (CCA)[34] to the FC, GMV, or their concatenation (COMB) matrices. CCA maximizes correlations between a pair of canonical components, which is a weighted summation of the input matrices. The objective of CCA is well suited to this problem, because parent-child identification was conducted based on the correlation coefficient between two pairs. We also applied principal component analysis (PCA) for reducing noise in the dataset before applying CCA, which is considered a conventional approach in the field of neuroimaging[11,15,35]. Weights

of CCA, PCA, and the dimensions of PCA were determined by nested cross-validation (CV), as follows. The dimension of CCA was not tuned and fixed to the number of principal components.

We first split all parent-child pairs into 10 sets (outer-CV). We then selected nine sub-sets (outer-training-set) and left one sub-set as a held-out set (outer-test-set). We further split outer-training-set into five sub-sets (inner-CV) and conducted identification analyses within this inner-CV for determining the hyper-parameter of our analysis: the dimension of PCA.

In the inner-CV, we selected four sub-sets (inner-training-set) and left one sub-set as a held-out set (inner-test-set). Using a brain matrix (FC, GMV or COMB) of children at age 11 in the inner-training-set, we applied PCA and estimated the transformation matrix. We then applied the transformation matrix to the brain matrices of children at age 13 and their parents in the inner-training-set, and brain matrices of children at age 11, children at age 13, and their parents in the inner-test-set. We next applied CCA to the obtained principal components of parent-child pairs in the inner-training-set, and the obtained transformation matrix was applied to the principal components of parent-child pairs in the inner-test-set. The obtained canonical components were used as an input for the identification analyses. By using only the inner-test-set, we conducted identification in the same manner as described above. We repeated this procedure five times (5-fold CV) and obtained inner-CV accuracy by averaging the accuracies across five sub-sets.

In the outer-CV, we used the dimensions of PCA that performed best in the inner-CV. The dimensions of PCA were tuned by choosing the best value from {95%, 90%, 85%, and 80% of variance explained}. Transformation matrices of PCA and CCA were estimated using the outer-training-set in the same manner as inner-CV. The estimated transformation matrices were then applied to the outer-test-set, and the obtained canonical components were used for identification analyses. Identification was conducted using only the outer-test-set. We repeated this procedure 10 times (10-fold CV) and the final accuracy was obtained by averaging the accuracies across 10 sub-sets.

Behavioral correlation

To investigate whether parent-child brain similarity is relevant to behavior, we defined “neural

527 similarity" and "behavioral similarity" as described below. We then calculated Spearman's
528 rank correlation coefficients between neural similarity and behavioral similarity across pairs.

529 We defined neural similarity as the correlation coefficient between brain
530 information (COMB with CCA) of parents and their children. As in the previous analyses, we
531 calculated the neural similarity for every 10 sub-networks and the whole-brain.

532 For behavioral similarity, we used the difference in fundamental cognitive measures
533 of intelligence between parents and their children. In the pn-TTC protocol, a child's
534 intelligence was estimated from the four-item short version of Wechsler Intelligence Scale for
535 Children III[51] (WISC-III; 110.99 ± 13.14, mean ± s.t.d) at age 12. Parent's intelligence was
536 assessed using the 25-item short version of the Japanese Adult Reading Test[52,53] (108.05 ±
537 8.13, mean ± s.t.d) when their children were 10 years old. Both of the scores were transformed
538 using inverse Gaussian transformation to enforce Gaussianity[54]. We defined behavioral
539 similarities as the absolute difference between parents' and their children's intelligence scores.
540 For interpretability, we multiplied minus one with the absolute difference.

541 For the analysis in Figure 4b, we performed bootstrapping to estimate the
542 confidence interval of accuracy: we randomly subsampled 90% of the subjects in each
543 iteration and calculated Spearman's rank correlation coefficients. The process was repeated
544 1,000 times. We also used 1,000-times permutation testing to generate a null distribution, by
545 randomly shuffling the parent-child mapping.

546

References

1. de Graaf, P. M. & Kalmijn, M. Trends in the Intergenerational Transmission of Cultural and Economic Status. *Acta Sociol.* **44**, 51–66 (2001).
2. Deary, I. J., Spinath, F. M. & Bates, T. C. Genetics of intelligence. *Eur. J. Hum. Genet.* **14**, 690–700 (2006).
3. Grønhøj, A. & Thøgersen, J. Like father, like son? Intergenerational transmission of values, attitudes, and behaviours in the environmental domain. *J. Environ. Psychol.* **29**, 414–421 (2009).
4. Kalmuss, D. The intergenerational transmission of marital aggression. *J. Marriage Fam.* 11–19 (1984).
5. Corak, M. Income inequality, equality of opportunity, and intergenerational mobility. *J. Econ. Perspect.* **27**, 79–102 (2013).
6. Miller, R. B. & Glass, J. Parent-child attitude similarity across the life course. *J. Marriage Fam.* 991–997 (1989).
7. Dubois, J. & Adolphs, R. Building a Science of Individual Differences from fMRI. *Trends Cogn. Sci.* **20**, 1–19 (2016).
8. Biswal, B. B. *et al.* Toward discovery science of human brain function. *Proc. Natl. Acad. Sci. U. S. A.* **107**, 4734–9 (2010).
9. Finn, E. S. *et al.* Functional connectome fingerprinting: identifying individuals using patterns of brain connectivity. *Nat. Neurosci.* **18**, 1–11 (2015).
10. Rosenberg, M. D. *et al.* A neuromarker of sustained attention from whole-brain functional connectivity. *Nat. Neurosci.* **19**, 165–71 (2016).
11. Takagi, Y., Hirayama, J. ichiro & Tanaka, S. C. State-unspecific patterns of whole-brain functional connectivity from resting and multiple task states predict stable individual traits. *Neuroimage* **201**, 116036 (2019).
12. Takagi, Y. *et al.* A common brain network among state, trait, and pathological anxiety from whole-brain functional connectivity. *Neuroimage* **172**, 506–516 (2018).
13. van den Heuvel, M. P., Stam, C. J., Kahn, R. S. & Hulshoff Pol, H. E. Efficiency of functional brain networks and intellectual performance. *J. Neurosci.* **29**, 7619–24 (2009).
14. Fox, M. D. & Greicius, M. Clinical applications of resting state functional connectivity. *Front. Syst. Neurosci.* **4**, 19 (2010).
15. Takagi, Y. *et al.* A neural marker of obsessive-compulsive disorder from whole-brain functional connectivity. *Sci. Rep.* **7**, 7538 (2017).

16. Yamashita, A. *et al. Harmonization of resting-state functional MRI data across multiple imaging sites via the separation of site differences into sampling bias and measurement bias*. *PLoS Biology* **17**, (2019).
17. Yahata, N. *et al.* A small number of abnormal brain connections predicts adult autism spectrum disorder. *Nat. Commun.* **7**, (2016).
18. Kanai, R. & Rees, G. The structural basis of inter-individual differences in human behaviour and cognition. *Nat. Rev. Neurosci.* **12**, 231–242 (2011).
19. Busch, V., Schuierer, G., Bogdahn, U. & May, A. Changes in grey matter induced by training Newly honed juggling skills show up as a transient feature on a brain-imaging scan . *Nature* **427**, 311–312 (2004).
20. Duncan, J. *et al.* A neural basis for general intelligence. *Science (80-.).* **289**, 457–460 (2000).
21. Okada, N. *et al.* Smaller anterior subgenual cingulate volume mediates the effect of girls' early sexual maturation on negative psychobehavioral outcome. *Neuroimage* **209**, 116478 (2020).
22. Kasai, K. *et al.* Progressive decrease of left superior temporal gyrus gray matter volume in patients with first-episode schizophrenia. *Am. J. Psychiatry* **160**, 156–164 (2003).
23. Steiger, V. R. *et al.* Pattern of structural brain changes in social anxiety disorder after cognitive behavioral group therapy: A longitudinal multimodal MRI study. *Mol. Psychiatry* **22**, 1164–1171 (2017).
24. Alexander-Bloch, A., Raznahan, A., Bullmore, E. & Giedd, J. The convergence of maturational change and structural covariance in human cortical networks. *J. Neurosci.* **33**, 2889–2899 (2013).
25. Lee, T. H., Miernicki, M. E. & Telzer, E. H. Families that fire together smile together: Resting state connectome similarity and daily emotional synchrony in parent-child dyads. *Neuroimage* **152**, 31–37 (2017).
26. Quiñones-Camacho, L. E. *et al.* Parent–child neural synchrony: a novel approach to elucidating dyadic correlates of preschool irritability. *J. Child Psychol. Psychiatry Allied Discip.* (2019). doi:10.1111/jcpp.13165
27. Reindl, V., Gerloff, C., Scharke, W. & Konrad, K. Brain-to-brain synchrony in parent-child dyads and the relationship with emotion regulation revealed by fNIRS-based hyperscanning. *Neuroimage* **178**, 493–502 (2018).
28. Yamagata, B. *et al.* Female-specific intergenerational transmission patterns of the human corticolimbic circuitry. *J. Neurosci.* **36**, 1254–1260 (2016).
29. Ando, S. *et al.* Cohort Profile: The Tokyo Teen Cohort study (TTC). *Int. J. Epidemiol.* **48**,

(2019).
30. Okada, N. *et al.* Population-neuroscience study of the Tokyo TEEN Cohort (pn-TTC): Cohort longitudinal study to explore the neurobiological substrates of adolescent psychological and behavioral development. *Psychiatry Clin. Neurosci.* **73**, 231–242 (2019).
31. Shen, X., Tokoglu, F., Papademetris, X. & Constable, R. T. Groupwise whole-brain parcellation from resting-state fMRI data for network node identification. *Neuroimage* **82**, 403–415 (2013).
32. Power, J. D., Barnes, K. A., Snyder, A. Z., Schlaggar, B. L. & Petersen, S. E. Spurious but systematic correlations in functional connectivity MRI networks arise from subject motion. *Neuroimage* **59**, 2142–2154 (2012).
33. Horien, C., Shen, X., Scheinost, D. & Constable, R. T. The individual functional connectome is unique and stable over months to years. *Neuroimage* **189**, 676–687 (2019).
34. Hotelling, H. Relations between two sets of variates. *Biometrika* **28**, 321–377 (1936).
35. Smith, S. M. *et al.* A positive-negative mode of population covariation links brain connectivity, demographics and behavior. *Nat. Neurosci.* **18**, 1–7 (2015).
36. Arain, M. *et al.* Maturation of the adolescent brain. *Neuropsychiatr. Dis. Treat.* **9**, 449–461 (2013).
37. Kumar, K., Toews, M., Chauvin, L., Colliot, O. & Desrosiers, C. Multi-modal brain fingerprinting: A manifold approximation based framework. *Neuroimage* **183**, 212–226 (2018).
38. Gottfredson, L. S. Why g matters: The complexity of everyday life. *Intelligence* **24**, 79–132 (1997).
39. Whitley, E., Gale, C. R., Deary, I. J., Kivimaki, M. & Batty, G. D. Association of maternal and paternal IQ with offspring conduct, emotional, and attention problem scores: Transgenerational evidence from the 1958 British birth cohort study. *Arch. Gen. Psychiatry* **68**, 1032–1038 (2011).
40. Colclough, G. L. *et al.* The heritability of multi-modal connectivity in human brain activity. *Elife* **6**, 1–19 (2017).
41. Miranda-Dominguez, O. *et al.* Heritability of the human connectome: A connectotyping study. *Netw. Neurosci.* **2**, 175–199 (2018).
42. Yeh, F. C. *et al.* Quantifying Differences and Similarities in Whole-Brain White Matter Architecture Using Local Connectome Fingerprints. *PLoS Comput. Biol.* **12**, 1–17 (2016).
43. Kumar, K., Desrosiers, C., Siddiqi, K., Colliot, O. & Toews, M. Fiberprint: A subject

fingerprint based on sparse code pooling for white matter fiber analysis. *Neuroimage* **158**, 242–259 (2017).

44. Valizadeh, S. A., Liem, F., Mérillat, S., Hänggi, J. & Jäncke, L. Identification of individual subjects on the basis of their brain anatomical features. *Sci. Rep.* **8**, 1–9 (2018).

45. Wachinger, C., Golland, P., Kremen, W., Fischl, B. & Reuter, M. BrainPrint: A discriminative characterization of brain morphology. *Neuroimage* **109**, 232–248 (2015).

46. Grotevant, H. D. & Cooper, C. R. Individuation in family relationships. *Hum. Dev.* **29**, 82–100 (1986).

47. Zuo, X. N. *et al.* Human Connectomics across the Life Span. *Trends Cogn. Sci.* **21**, 32–45 (2017).

48. Rosenberg, M. D., Casey, B. J. & Holmes, A. J. Prediction complements explanation in understanding the developing brain. *Nat. Commun.* 1–13 (2018). doi:10.1038/s41467-018-02887-9

49. Honey, C. J. *et al.* Predicting human resting-state functional connectivity from structural connectivity. *Proc. Natl. Acad. Sci. U. S. A.* **106**, 2035–2040 (2009).

50. Gong, G., He, Y., Chen, Z. J. & Evans, A. C. Convergence and divergence of thickness correlations with diffusion connections across the human cerebral cortex. *Neuroimage* **59**, 1239–1248 (2012).

51. Kaufman, A. S. *Intelligent testing with the WISC-III.* (John Wiley & Sons, 1994).

52. Hirata-Mogi, S. *et al.* Reliability of a paper-and-pencil version of the Japanese Adult Reading Test short version. *Psychiatry Clin. Neurosci.* **70**, 362 (2016).

53. Matsuoka, K., Uno, M., Kasai, K., Koyama, K. & Kim, Y. Estimation of premorbid IQ in individuals with Alzheimer's disease using Japanese ideographic script (Kanji) compound words: Japanese version of National Adult Reading Test. *Psychiatry Clin. Neurosci.* **60**, 332–339 (2006).

54. der Waerden, B. L. & van der Waerden, B. Order tests for the two-sample problem and their power. *Indag. Math.* **14**, 253–458 (1952).

Figures

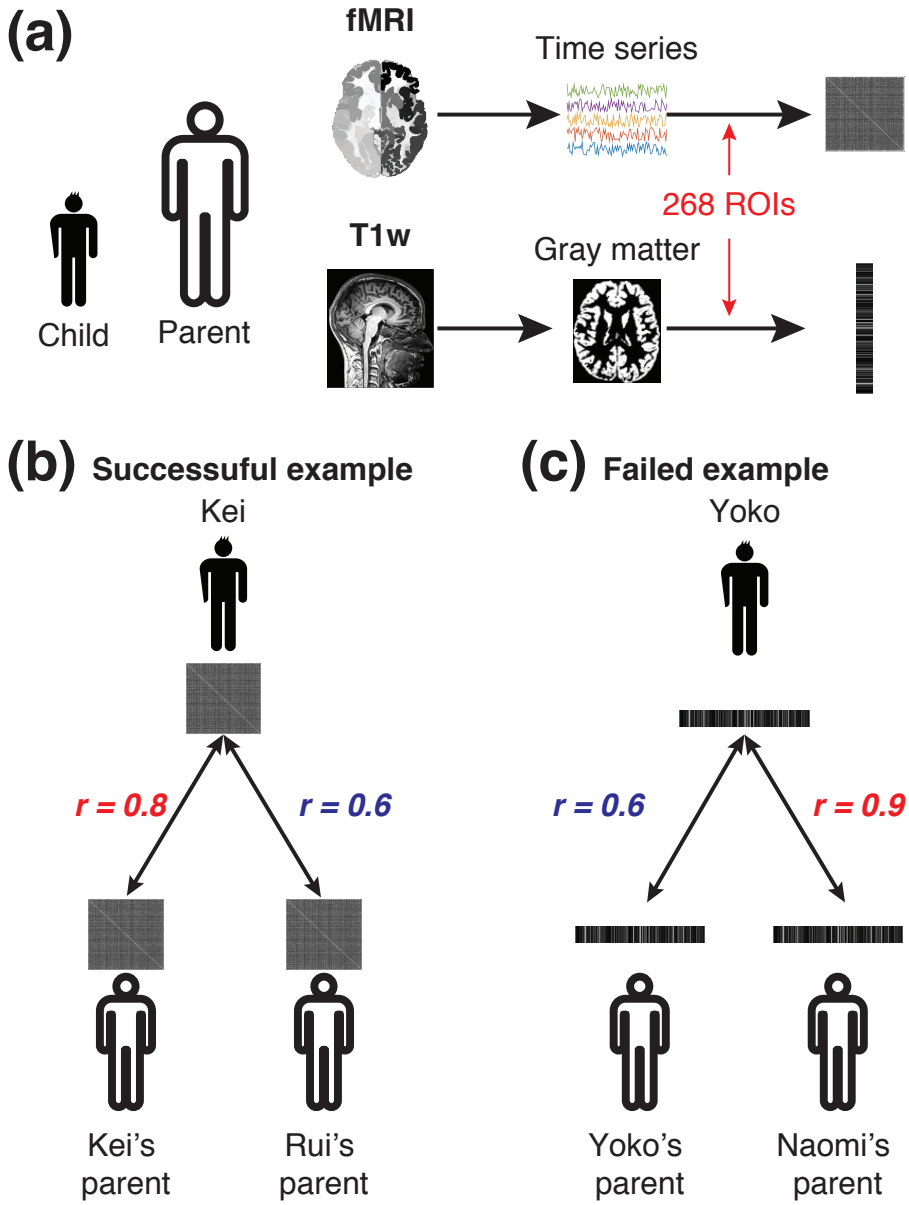

Figure 1: Analysis procedure. (**a**) We employed a dataset obtained from the "population-neuroscience study of the Tokyo TEEN Cohort (pn-TTC)" study, which consists of resting-state fMRI and T1w images of parents and their children. To obtain a functional connectivity (FC) matrix, signals were extracted from all subjects using resting-state fMRI data from whole-brain regions of interest (ROIs; N = 268). The signals were then turned into an FC matrix via covariance estimation. To obtain gray matter volume (GMV) vectors, T1w images were first segmented into gray matter, white matter, and cerebrospinal fluid. Using the gray matter, GMV of each ROI was obtained by averaging values within the ROI. We used the same 268 ROIs as in the FC. **(b)** If the Pearson's correlation coefficient between a parent and the parent's child was higher than that of the child and a randomly selected parent of another child, it was recorded as a successful identification. **(c)** In contrast, if the Pearson's correlation coefficient between a parent and the parent's child was smaller than that of the child and a randomly selected parent, it was recorded as a failed identification.

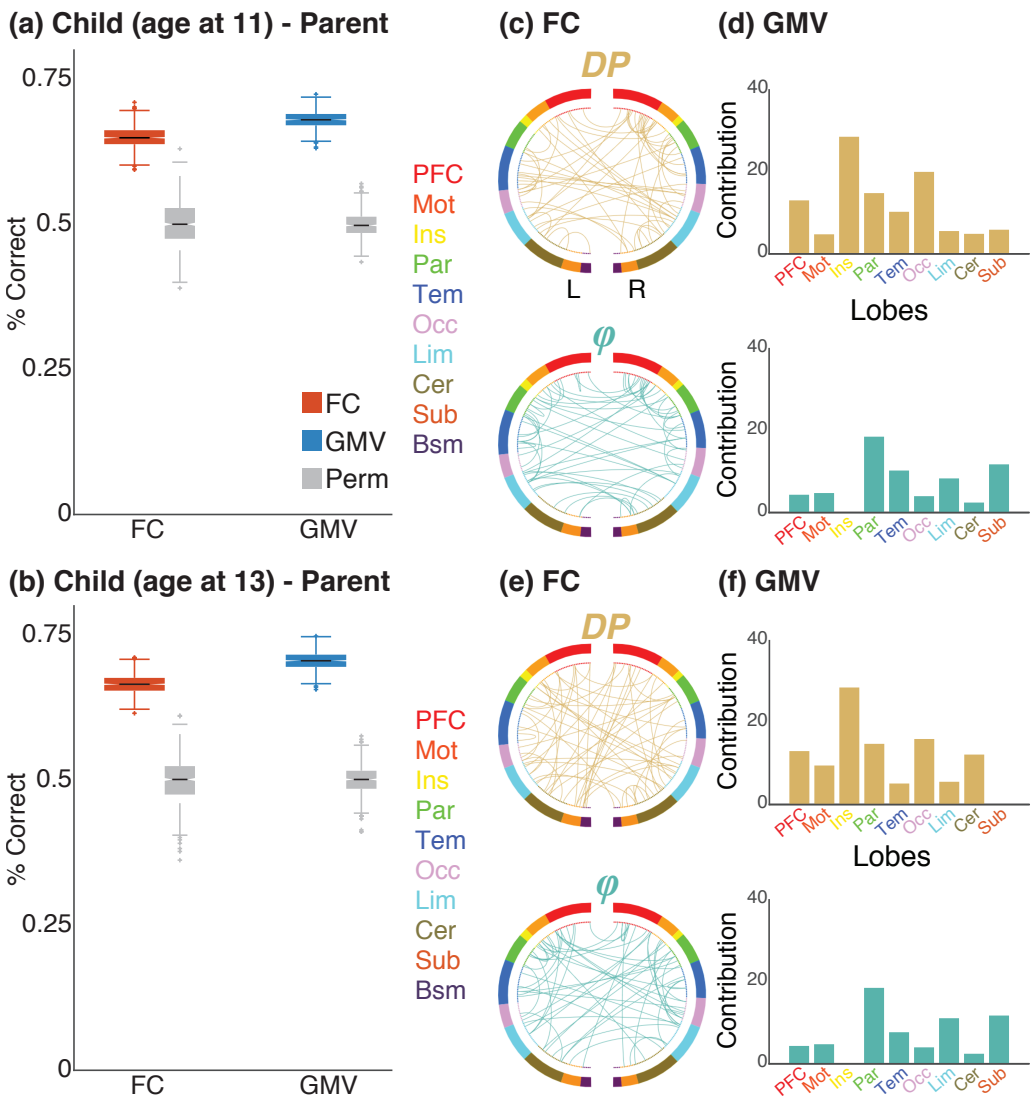

Figure 2: Box plots of parent-child identification accuracy and factors affecting accuracy for **(a)** children at age 11 and **(b)** at age 13 using whole-brain (268-node) for functional connectivity (FC: red box) and gray matter volume (GMV: blue box). Directly to the right of these boxes (gray box) are the results of the 1,000-times permutation testing. The black line indicates the median. The bottom and top edges of the box indicate the 25th and 75th percentiles obtained via bootstrapping, respectively. The crosses denote outliers, and the whiskers extend to the most extreme data points not considered outliers. **(c–f)** Factors affecting identification accuracy. For FC, the top 99.75th percentile of differential power (DP: highly discriminative; yellow) edges and group consistency (Φ: highly similar, or least helpful; green) edges are shown (circle plot; in which nodes are grouped according to anatomic location). For GMV, the top 90th percentile ROIs of DP and Φ were calculated, then normalized by dividing the number of ROIs in each anatomical group (bar plot). A legend indicating the approximate anatomical "lobe" is shown. PFC, prefrontal; Mot, motor; Ins, insula; Par, parietal; Tem, temporal; Occ, occipital; Lim, limbic (including cingulate cortex, amygdala, and hippocampus); Cer, cerebellum; Sub, subcortical (including thalamus and striatum); Bsm, brainstem; L, left hemisphere; R, right hemisphere.

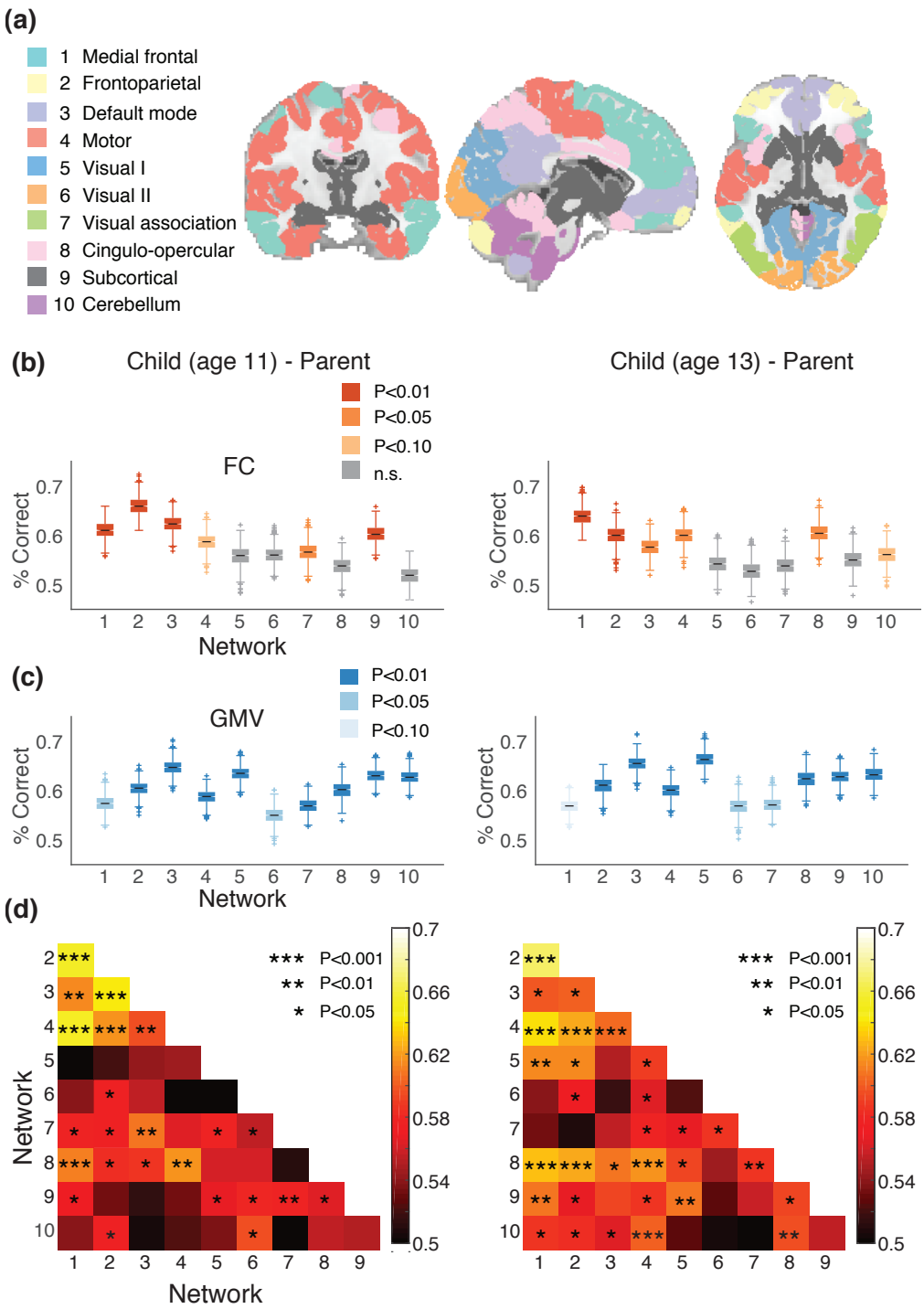

Figure 3: Network-based identification accuracy. (**a**) We utilized a 268-node functional atlas. Nodes were further grouped into the 10 functional networks. Network names are shown to the left. (**b**) Box plots of accuracies using only within-network edges of FC analysis (networks 1–10; indicated below the x-axis of each graph) and (**c**) within-network nodes of GMV analysis. The black line indicates the median. The bottom and top edges of the box indicate the 25th and 75th percentiles, respectively. The crosses denote outliers, and the whiskers extend to the most extreme data points not considered outliers. (**d**) Between-network analyses using only the between-network edges. Statistical significance was assessed by comparing the distributions for each network obtained through bootstrapping. n.s. non-significant, uncorrected.

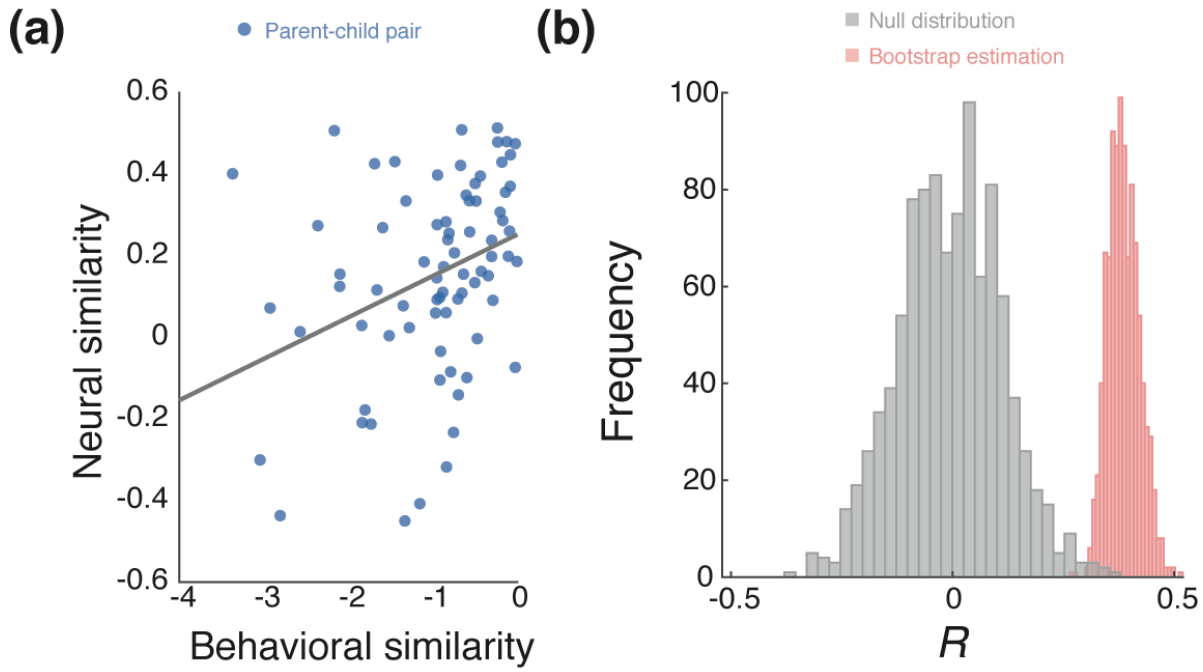

Figure 4: Relationship between neural similarity and behavioral similarity. (**a**) Parent-child neural similarity (correlation between parent-child brains) is positively correlated with their behavioral similarity (negative absolute difference between parent-child intelligence quotient [IQ] scores). (**b**) Correlation coefficients estimated via bootstrapping (red bar) and null distribution (gray bar) estimated via permutation are shown.

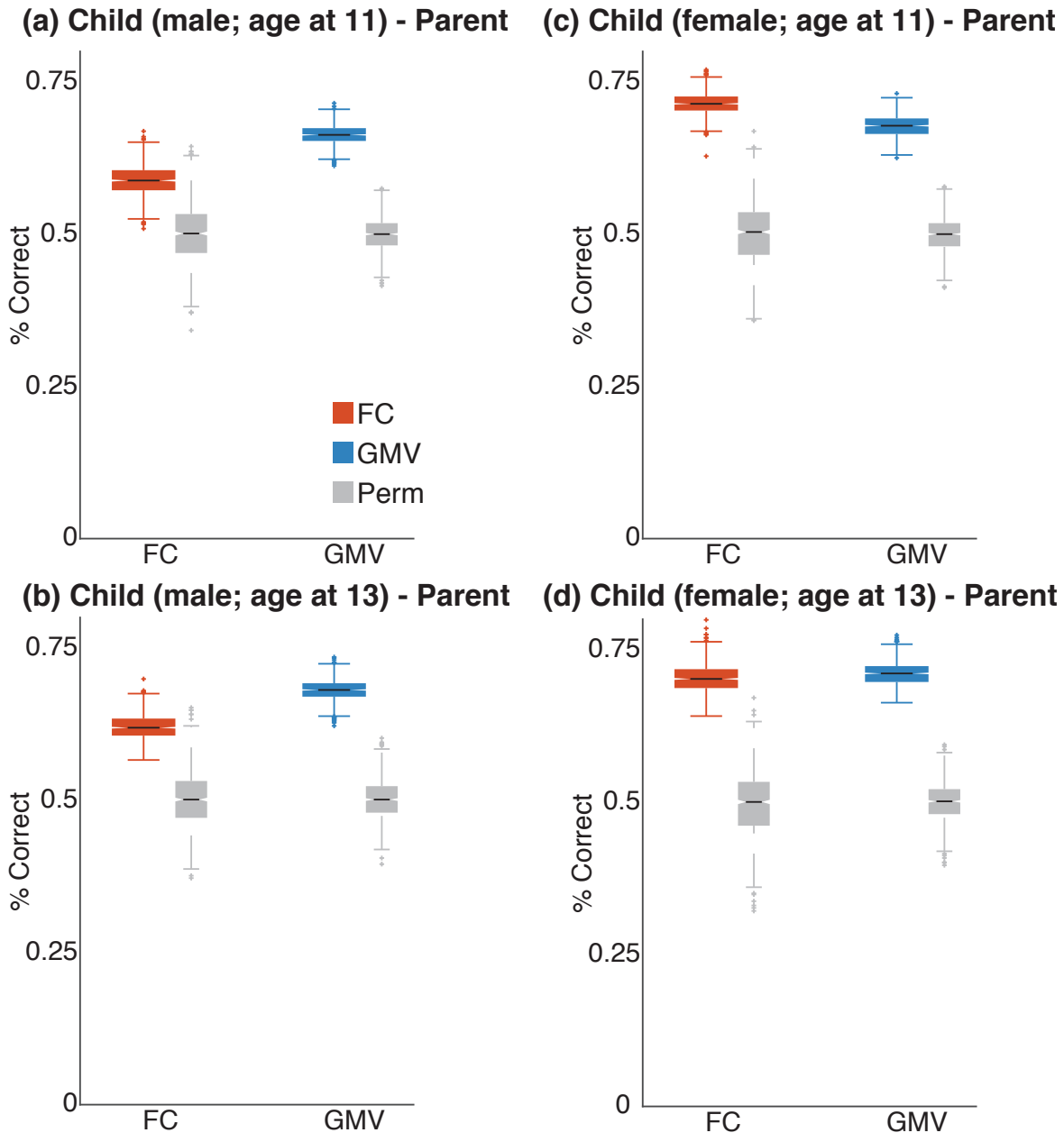

Supplementary Figure 1: Identification accuracies split by children's sex. Identification accuracies of FC for males (red boxes in **(a)** and **(b)**) were slightly lower than those for females (red boxes in **(c)** and **(d)**).

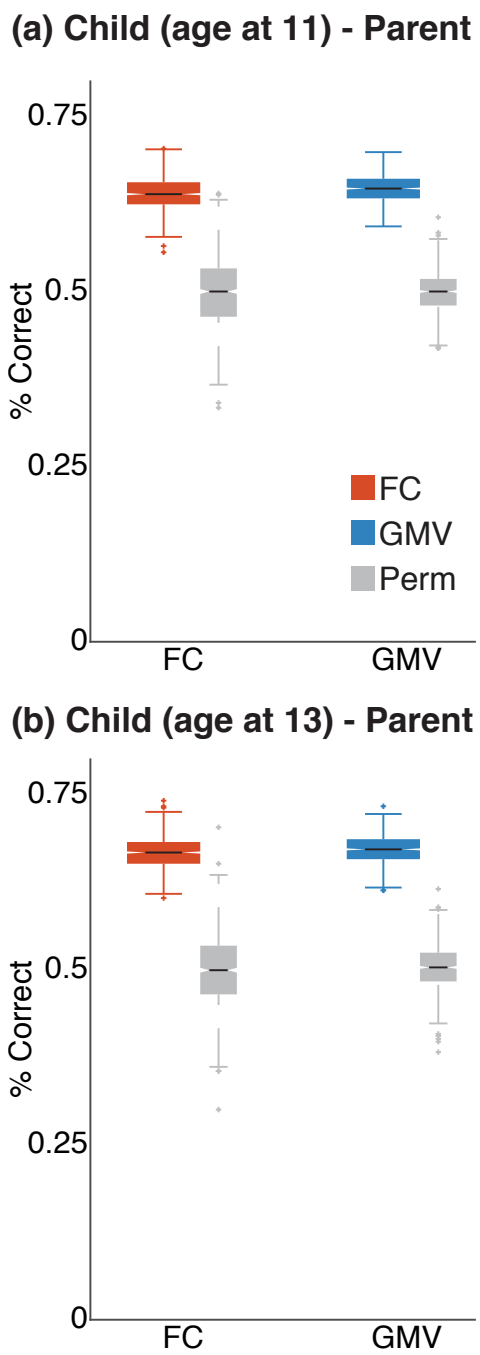

Supplementary Figure 2: Identification accuracies using only low-movement subjects. We confirmed that qualitatively similar results were obtained when we excluded children whose head movements were in the top 25%, either at age 11 or at age 13, resulting in the inclusion of 41.25% of the total sample.

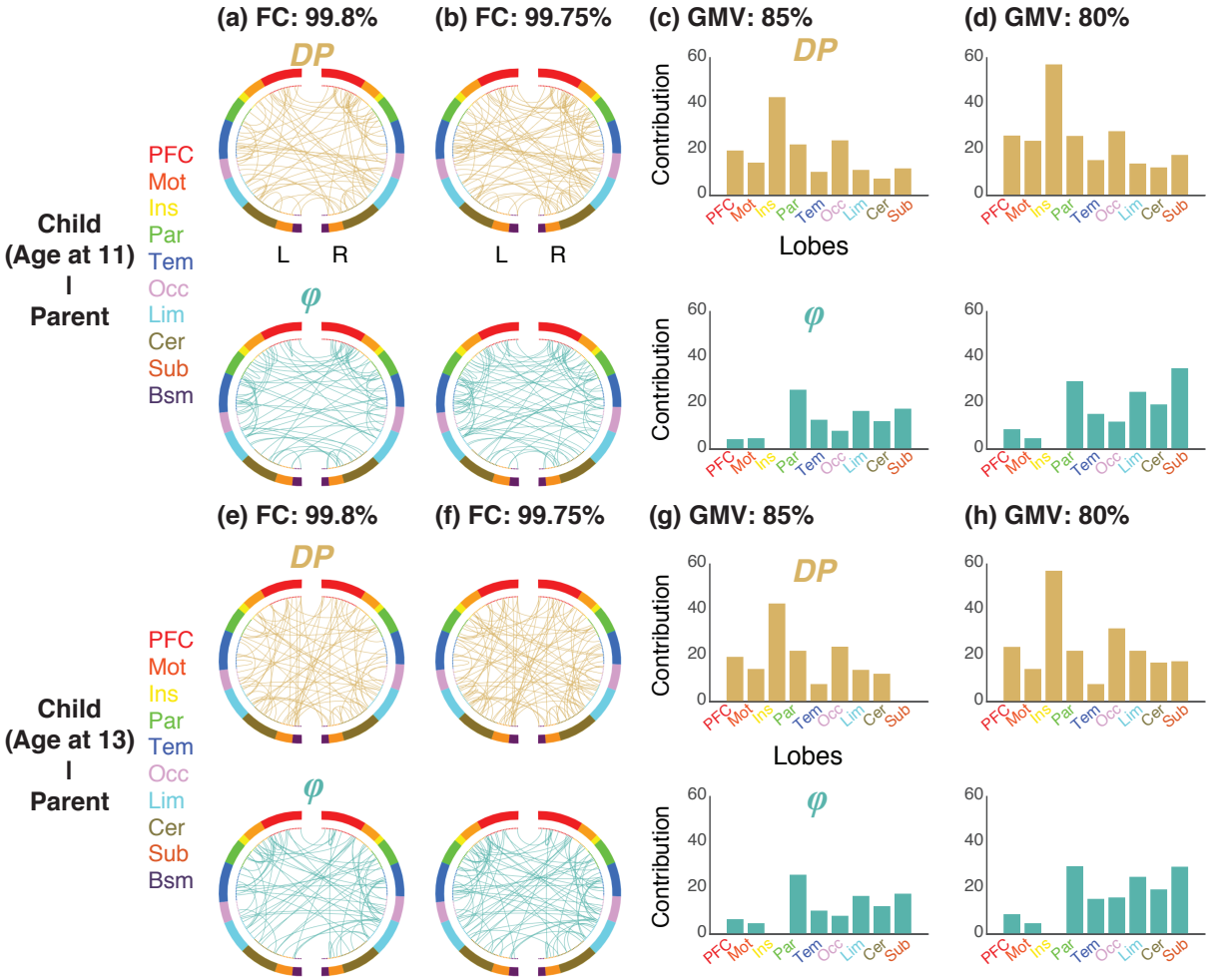

Supplementary Figure 3: Overall patterns of edges/regions with high differential power (highly discriminative among subjects) and group consistency (highly similar among subjects) tended to be similar across different thresholds and across development (**(a)**-**(d)** child at age 11); **(e)**-**(h)** child at age 13). The figures show the results when the edges were thresholded at the 99.8th and 99.75th percentiles for FC, and regions were thresholded at the 85th, 80th percentiles for GMV. For each threshold, a circle plot (FC) and a bar graph (GMV) are shown, in which nodes are grouped according to anatomical location.

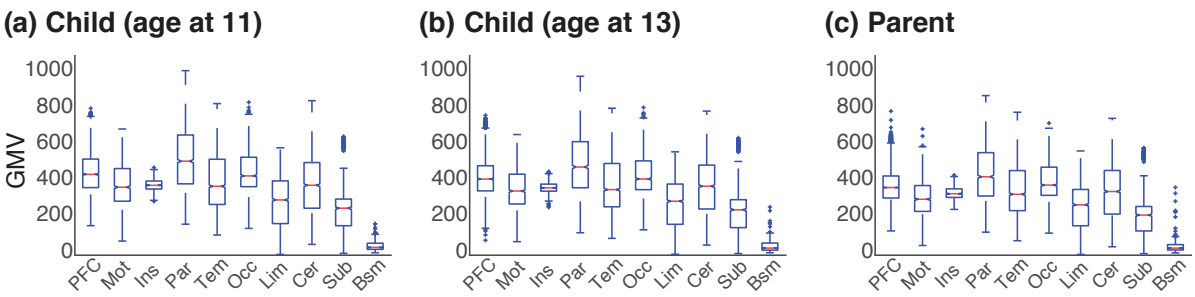

Supplementary Figure 4: Box plots of signal strength of each lobule for GMV. The red line indicates the median. The bottom and top edges of the box indicate the 25th and 75th percentiles, respectively. The crosses denote outliers, and the whiskers extend to the most extreme data points not considered outliers. The brainstem (the right-most boxes in each figure) exhibited much lower signal strength compared with the other lobules. Mean ± s.e.m is shown.

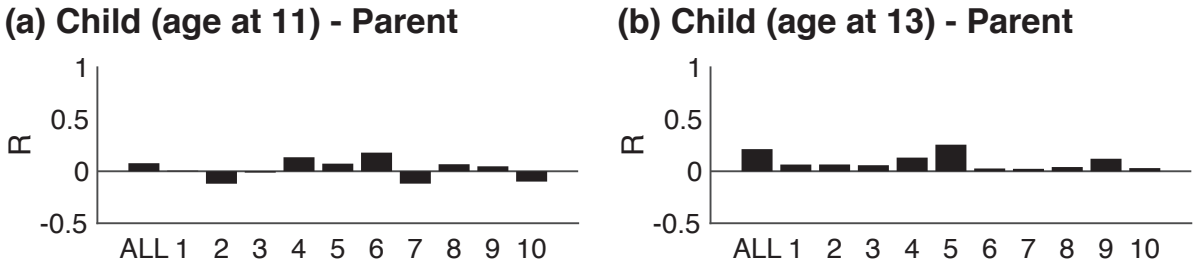

Supplementary Figure 5: For each sub-network (1–10: sub-networks shown in Figure 3a) and whole-brain (ALL), we calculated the Pearson's correlation coefficient between parent-child brain similarities defined by FC and those defined by GMV across all parent-child pairs. We found that they exhibited relatively low correlations in general, suggesting that they contained independent information for identification.

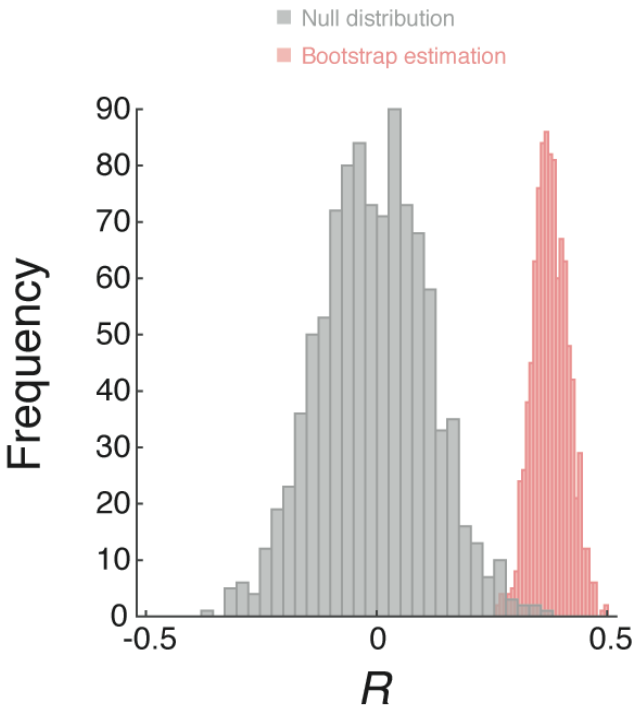

Supplementary Figure 6: Partial correlation of neural similarity and behavioral similarity. Here we controlled the average FD of children at age 11, children at age 13, and parents.

Tables

	N	Age[a] (mean ± s.t.d)	Gender (Male/Female)	Intelligent Quotient[b] (mean ± s.t.d)
Child age at 11	84	11.59±0.66	45/39	-
Child age at 13		13.63±0.62		110.99±13.14
Parent		43.35±3.95	3/81	108.05±8.13

Table 1: Demographic data. [a] Age of parents when their children were 11 years old are shown. [b] For child's IQ, we used the four-item short version of the Wechsler Intelligence Scale for Children III (WISC-III) obtained at age 12. For parent's IQ, we used 25-item short version of the Japanese Adult Reading Test, obtained when their children were 10 years old.

Network	Pair	FC	GMV	COMB	COMB (CCA)
ALL	C11-P	64.99 [61.70,68.70]	68.02 [65.10,70.70]	**68.05 [65.20,71.00]**	**82.54 [78.79,86.24]**
	C13-P	66.52 [63.50,69.70]	70.54 [67.60,73.40]	**70.80 [67.80,73.80]**	**79.06 [75.22,83.12]**
MF	C11-P	**61.05 [57.20,64.80]**	57.42 [54.40,60.60]	57.51 [54.50,60.60]	**62.84 [56.50,68.55]**
	C13-P	**63.85 [60.30,67.50]**	56.85 [54.20,59.40]	56.86 [54.00,59.60]	**60.32 [54.66,65.64]**
FP	C11-P	**65.95 [62.40,69.60]**	60.43 [57.60,63.20]	61.22 [58.50,63.70]	**64.88 [59.22,70.22]**
	C13-P	59.99 [56.00,63.40]	60.99 [57.30,64.00]	**62.05 [58.70,64.80]**	**64.17 [58.63,69.14]**
DMN	C11-P	62.29 [58.70,65.50]	64.75 [61.90,67.60]	**65.25 [62.40,68.00]**	**71.99 [66.42,77.39]**
	C13-P	57.66 [54.40,61.00]	65.45 [62.10,68.30]	**65.48 [62.40,68.50]**	**68.85 [63.14,74.48]**
Mot	C11-P	58.70 [55.40,62.30]	58.73 [55.70,61.40]	**58.92 [55.80,61.80]**	**68.21 [62.81,73.29]**
	C13-P	60.00 [56.30,63.70]	60.04 [56.90,62.90]	**60.13 [57.10,63.30]**	**65.66 [60.24,70.98]**
Vis I	C11-P	55.81 [51.60,59.60]	63.45 [60.70,66.10]	**64.06 [61.30,66.90]**	**67.33 [61.93,72.29]**
	C13-P	54.22 [50.30,58.10]	66.32 [63.40,69.30]	**66.64 [63.50,69.50]**	**66.93 [61.11,72.20]**
Vis II	C11-P	56.03 [52.90,59.50]	55.00 [52.00,58.20]	**57.55 [54.60,60.80]**	**59.70 [53.72,65.17]**
	C13-P	52.78 [49.20,57.00]	56.82 [53.50,60.20]	**59.19 [55.50,62.80]**	**59.07 [53.06,65.05]**
Vis A	C11-P	56.69 [53.00,60.60]	**56.93 [53.90,59.90]**	56.80 [54.00,59.40]	**62.67 [56.95,68.21]**
	C13-P	53.83 [50.00,57.40]	**57.14 [54.10,60.20]**	56.46 [53.40,59.40]	**59.99 [53.77,65.77]**
Cing	C11-P	53.77 [50.10,57.30]	60.13 [56.50,63.30]	**60.36 [56.90,63.50]**	**68.05 [62.57,73.49]**
	C13-P	60.49 [56.70,64.10]	62.36 [58.80,65.60]	**62.41 [59.20,65.70]**	**65.81 [60.25,70.99]**
Sub	C11-P	60.28 [57.20,63.60]	**63.07 [60.40,65.80]**	63.01 [60.30,65.60]	**75.64 [70.96,80.25]**
	C13-P	55.01 [51.40,59.00]	62.80 [59.90,65.80]	**62.90 [60.10,65.70]**	**73.91 [68.74,78.75]**
Cer	C11-P	51.89 [48.20,55.60]	**62.76 [59.90,65.60]**	61.89 [59.20,64.60]	**75.89 [71.08,80.53]**
	C13-P	56.14 [52.50,60.00]	**63.26 [60.10,66.50]**	62.55 [59.60,65.60]	**73.53 [68.25,78.34]**
# best		2	0	1	19
# 2nd best		1	5	13	3

Table 2: Accuracy of identification of children at age 11 and their parents (C11-P), and children at age 13 and their parents (C13-P) using different sub-networks and whole-brain data. We used functional connectivity (FC), gray matter volume (GMV), or a combination of both (COMB). We also applied canonical correlation analysis (CCA) to COMB. Means and 95% confidence intervals estimated via 1,000 times bootstrapping are shown. **Bold red** text indicates the best performance, and **bold underlined** text indicates the second-best performance. MF, medial frontal; FP, frontoparietal; DMN, default mode network; Mot, motor; Vis I, visual I; Vis II, visual II; Vis A, visual association; Cing, cingulo-opercular; Sub, subcortical; Cer, cerebellum.

Network	Pair	MOTION	FC	GMV	COMB	FC (CCA)	GMV (CCA)	COMB (CCA)
ALL	C11-P	50.15 [46.90,53.10]	64.99 [61.70,68.70]	68.02 [65.10,70.70]	68.05 [65.20,71.00]	56.53 [51.84,61.29]	**82.01 [77.90,85.90]**	**82.54 [78.79,86.24]**
	C13-P	47.55 [44.30,50.80]	66.52 [63.50,69.70]	70.54 [67.60,73.40]	70.80 [67.80,73.80]	57.86 [53.60,62.47]	**78.50 [74.22,82.67]**	**79.06 [75.22,83.12]**
MF	C11-P	-	61.05 [57.20,64.80]	57.42 [54.40,60.60]	57.51 [54.50,60.60]	61.81 [56.67,67.03]	**62.98 [57.25,68.91]**	**62.84 [56.50,68.55]**
	C13-P	-	**63.85 [60.30,67.50]**	56.85 [54.20,59.40]	56.86 [54.00,59.60]	62.59 [57.38,67.53]	60.31 [54.54,65.91]	**60.32 [54.66,65.64]**
FP	C11-P	-	**65.95 [62.40,69.60]**	60.43 [57.60,63.20]	61.22 [58.50,63.70]	59.54 [54.28,64.82]	64.71 [59.00,70.41]	**64.88 [59.22,70.22]**
	C13-P	-	59.99 [56.00,63.40]	60.99 [57.30,64.00]	62.05 [58.70,64.80]	54.87 [48.86,60.68]	**64.10 [58.70,69.24]**	**64.17 [58.63,69.14]**
DMN	C11-P	-	62.29 [58.70,65.50]	64.75 [61.90,67.60]	65.25 [62.40,68.00]	58.08 [52.95,63.28]	**71.04 [65.69,76.14]**	**71.99 [66.42,77.39]**
	C13-P	-	57.66 [54.40,61.00]	65.45 [62.10,68.30]	65.48 [62.40,68.50]	54.41 [48.67,60.08]	**67.88 [62.43,73.06]**	**68.85 [63.14,74.48]**
Mot	C11-P	-	58.70 [55.40,62.30]	58.73 [55.70,61.40]	58.92 [55.80,61.80]	55.65 [50.66,60.41]	**66.42 [60.85,71.59]**	**68.21 [62.81,73.29]**
	C13-P	-	60.00 [56.30,63.70]	60.04 [56.90,62.90]	60.13 [57.10,63.30]	58.16 [52.57,63.70]	**64.06 [58.50,69.23]**	**65.66 [60.24,70.98]**
Vis I	C11-P	-	55.81 [51.60,59.60]	63.45 [60.70,66.10]	64.06 [61.30,66.90]	55.05 [49.75,60.65]	**67.54 [61.60,72.56]**	**67.33 [61.93,72.29]**
	C13-P	-	54.22 [50.30,58.10]	66.32 [63.40,69.30]	66.64 [63.50,69.50]	53.01 [47.61,58.40]	**67.05 [61.12,73.06]**	**66.93 [61.11,72.20]**
Vis II	C11-P	-	56.03 [52.90,59.50]	55.00 [52.00,58.20]	57.55 [54.60,60.80]	54.47 [49.07,60.33]	**59.71 [53.63,65.59]**	**59.70 [53.72,65.17]**
	C13-P	-	52.78 [49.20,57.00]	56.82 [53.50,60.20]	59.19 [55.50,62.80]	54.32 [48.67,60.08]	**59.14 [52.77,65.24]**	**59.07 [53.06,65.05]**
Vis A	C11-P	-	56.69 [53.00,60.60]	56.93 [53.90,59.90]	56.80 [54.00,59.40]	59.22 [53.30,65.08]	**62.27 [56.94,67.54]**	**62.67 [56.95,68.21]**
	C13-P	-	53.83 [50.00,57.40]	57.14 [54.10,60.20]	56.46 [53.40,59.40]	52.88 [47.20,58.68]	**59.50 [53.51,65.02]**	**59.99 [53.77,65.77]**
Cing	C11-P	-	53.77 [50.10,57.30]	60.13 [56.50,63.30]	60.36 [56.90,63.50]	50.54 [44.63,56.74]	**67.53 [62.06,72.67]**	**68.05 [62.57,73.49]**
	C13-P	-	60.49 [56.70,64.10]	62.36 [58.80,65.60]	62.41 [59.20,65.70]	58.93 [53.28,64.54]	**65.58 [60.44,70.88]**	**65.81 [60.25,70.99]**
Sub	C11-P	-	60.28 [57.20,63.60]	63.07 [60.40,65.80]	63.01 [60.30,65.60]	56.80 [51.39,62.02]	**74.90 [70.13,79.39]**	**75.64 [70.96,80.25]**
	C13-P	-	55.01 [51.40,59.00]	62.80 [59.90,65.80]	62.90 [60.10,65.70]	53.88 [48.31,59.19]	**73.66 [68.59,78.68]**	**73.91 [68.74,78.75]**
Cer	C11-P	-	51.89 [48.20,55.60]	62.76 [59.90,65.60]	61.89 [59.20,64.60]	53.47 [47.96,58.67]	**73.45 [68.29,78.54]**	**75.89 [71.08,80.53]**
	C13-P	-	56.14 [52.50,60.00]	63.26 [60.10,66.50]	62.55 [59.60,65.60]	55.54 [50.52,60.55]	**70.46 [64.91,75.60]**	**73.53 [68.25,78.34]**
# best		0	2	0	0	0	5	15
# 2nd best		0	0	0	0	0	15	7

Supplementary Table 1: Results of identification of children at age 11 and their parents (C11-P), and children at age 13 and their parents (C13-P) using different information. We used functional connectivity (FC), gray matter volume (GMV), or both (COMB). We also applied canonical correlation analysis (CCA) to COMB, FC, and GMV, respectively. To confirm that we could not conduct parent-child identification on the basis of the distribution of their frame-to-frame motion, we also used motion vectors (MOTION). Mean and 95% confidence intervals estimated via 1,000-times bootstrapping are shown. **Bold red** text indicates the best performance. **Bold underlined** text indicates the second-best performance. MF, medial frontal; FP, frontoparietal; DMN, default mode network; Mot, motor; Vis I, visual I; Vis II, visual II; Vis A, visual association; Cing, cingulo-opercular; Sub, subcortical; Cer, cerebellum.

Network name	Spearman's rho
Default Mode	0.3861 [0.4578,0.3232]
Motor	0.1373 [0.2084,0.0661]
Visual association	0.1125 [0.1867,0.0418]
Visual I	0.0987 [0.1676,0.0264]
Cerebellum	0.0918 [0.1646,0.0231]
Medial frontal	-0.0168 [0.0534,-0.0897]
Subcortical	-0.0278 [0.048,-0.1065]
All networks	-0.034 [0.0474,-0.1146]
Visual II	-0.0593 [0.0179,-0.1332]
Frontoparietal	-0.0611 [0.0091,-0.1405]
Cingulo-opercular	-0.0637 [0.0143,-0.14]

Supplementary Table 2: Relationship between neural similarity and behavioral similarity for all sub-networks. The order of networks is sorted by their correlation coefficients. The definition of each network is shown in Figure 3a. Mean and 95% confidence intervals obtained via 1,000-times bootstrapping are shown.